Trogoptosis as the mechanism whereby slan^{+}-monocytes kill therapeutic antibody-coated cancer cells

Giulia Finotti[1], Enrica Pietronigro[1], Camillo Balanzin[1], Silvia Lonardi[2], Gabriela Constantin[1], Mark P. Chao[3], Cristina Tecchio[4], William Vermi[2] and Marco A. Cassatella[1*]

[1]Section of General Pathology, Department of Medicine, University of Verona, Verona, Italy
[2]Section of Pathology, Department of Molecular and Translational Medicine, University of Brescia, Brescia, Italy.
[3]Stanford University, Division of Hematology, Stanford, CA 94305-5101, USA
[4]Section of Hematology and Bone Marrow Transplant Unit, Department of Medicine, University of Verona, Verona, Italy

Running title: CD20-,CD38- and CD47-mediated trogoptosis by slan^{+}-monocytes

Financial support: This work is supported by grants to: M.A.C. from Associazione Italiana per la Ricerca sul Cancro (AIRC, IG20339 and IG27613), Ministero dell'Istruzione, dell'Università e della Ricerca (MIUR-PRIN 20177J4E75_004); G.C. from European Research Council (ERC) Proof of Concept (grant nr. 101069397 NeutrAD); W.V. (AIRC IG-23179).

[*]**Corresponding Author:** Marco A. Cassatella, Section of General Pathology, Department of Medicine, University of Verona, Verona, Italy. *e-mail*: marco.cassatella@univr.it

The authors declare no potential conflicts of interest.

Keywords. slan^{+}-monocytes, trogocytosis/trogoptosis, ADCC, therapeutic antibodies, anti-CD47/Magrolimab

Word count: 5360
Figure count: 7 Figures, 5 Supplementary Figures, 3 Supplementary Videos

ABSTRACT

We have recently reported that human slan^{+}-monocytes, a major subset of non-classical CD14^{dim}CD16^{+}monocytes, exert a remarkable anti-CD20/Rituximab-mediated antibody-dependent cellular cytotoxicity (ADCC) of neoplastic B cells, as well as that slan^{+}-cells infiltrate lymphomas. Herein, by performing blocking experiments and flow cytometry analyses, as well as confocal microscopy and live-cell imaging assays, we extended the latter findings to other humanized antibodies, as well as deciphered the underlying effector mechanism(s). Specifically, we show that, after coculture with anti-CD20- and anti-CD38-coated target cells, slan^{+}-monocytes perform trogocytosis, a cell-cell contact dependent, antibody-mediated, process that triggers an active, mechanic, disruption of target cell membranes. Importantly, trogocytosis by slan^{+}-monocytes was found to lead to a necrotic type of target cell death, known as trogoptosis, that once initiated was partially sustained by endogenous TNFα. By the same types of analyses, we also report that slan^{+}-monocytes, unlike NK cells, perform a direct ADCC with all types of anti-CD47 antibodies used, independently from their IgG isotypes. The latter findings are noticeable as they unveil a potentially relevant contribution by slan^{+}-monocytes in mediating the therapeutic efficacy of anti-CD47 antibodies in the clinical practice, even more so when NK cells are exhausted or deficient in number. All in all, our observations shed new light on the cytotoxic mechanisms exerted by slan^{+}-monocytes in antibody-dependent tumor cell targeting, as well as advance our knowledge on how to expand our weapons for cancer therapy.

INTRODUCTION

Human monocytes, representing approximately 7-10 % of the peripheral leukocytes, are conventionally divided by flow cytometry into classical $CD14^{++}CD16^{-}$monocytes (~ 85 % of the total), intermediate $CD14^{+}CD16^{+}$monocytes (~ 5 %), and non-classical $CD14^{dim/-}CD16^{++}$monocytes (~ 10 %) (1). However, such a monocyte separation may result inaccurate due to the different approaches used to set a cut-off between CD14 and CD16 expression (2,3). Hence, an alternative identification of the $CD14^{dim/-}CD16^{++}$non-classical monocytes based on the detection of the 6-sulfo LacNac (slan) antigen by antibodies known as MDC8 and DD1/DD2 (4) has been recently proposed (5,6). As a result, the $slan^{+}$-monocytes emerge as 50/60 % of the non-classical $CD14^{dim/-}$ $CD16^{++}$monocytes. These cells have been widely characterized in terms of phenotype, functions, and disease localization, especially by Schäkel and coworkers (4,7), who initially named them as $slan^{+}$-dendritic cells (slanDCs) since endowed by a marked proinflammatory nature (given their production of IL12p70 and TNFα in remarkable amounts) and a potent capacity to induce T cell responses and Th1/Th17 cell polarization *in vitro* (6,7). However, with the advent of the "omics", slanDCs have been recognized to consist of a subset of non-classical $CD14^{dim/-}CD16^{++}$monocytes, as previously mentioned (6,7).

Our group has recently explored the role of $slan^{+}$-monocytes in lymphomas and solid cancer. We reported that $slan^{+}$-cells locate to metastatic tumor-draining lymph nodes (M-TDLNs) - but not to primary or metastatic tumors - where they align along the tumor front and adjacent to dead tumor cells, even appearing to contain dead cell bodies (8). We also showed that the circulating $slan^{+}$-monocyte compartment from patients with advanced colorectal cancer remains intact in terms of number and functions (i.e., TNFα and IL-12p70 production), suggesting that they are not developmentally/functionally hijacked or converted into immunosuppressive cells by growing tumors (8). In a following study, we could detect $slan^{+}$-cells in various types of non-Hodgkin lymphomas (NHL), particularly in diffuse large B cell lymphomas (DLBCL), in a status of either $slan^{+}$DC-like or macrophage-like cells (9). Notably, peripheral $slan^{+}$-monocytes were found to exert a remarkable anti-CD20/Rituximab (RTX)-mediated antibody-dependent cellular cytotoxicity (ADCC) of B cells from healthy donors (HD), neoplastic B cells from patients or B cell lines, at levels almost comparable to those exerted by NK cells (9). The latter cells, in fact, play a crucial role in tumor immunosurveillance, including in B cell lymphoma (10). Accordingly, an association between peripheral NK cell number decrease and non-Hodgkin's lymphoma development has been reported (11). Moreover, patients with low NK cell numbers are penalized by poor NK cell activities including RTX-dependent cytotoxicity (12). Hence, according to our previous findings

(9), it would be tempting to speculate that slan^{+}-monocytes might partially rescue NK cell-inability to mediate RTX-dependent ADCC.

In this study, not only we extend the knowledge on the therapeutic antibodies that slan^{+}-monocytes may use for ADCC, but also provide evidence that trogoptosis represents the final mechanism whereby slan^{+}-monocytes kill therapeutic antibody-coated tumor cells.

MATERIALS AND METHODS

Cell isolation and culture. Peripheral blood mononuclear cells (PBMCs) were isolated from buffy coats of healthy donors (HDs) by density centrifugation over Ficoll-Paque gradient (GE Healthcare) under endotoxin-free conditions (9). Natural killer (NK) cells and slan^{+}-monocytes were purified by, respectively, the EasySep^{TM} Human NK Cell Enrichment Kit (Stem Cell Technologies, > 95 % purity) and the slan (M-DC8)$^{+}$ Monocyte Isolation Kit (Miltenyi Biotec, > 96 % purity) (9), to be both used right after isolation in the various functional assays. In selected experiments, slan^{+}-monocytes were cultured *in vitro* for 5 days in the presence of 100 ng/mL IL-34 (R&D Systems) to generate slan^{+}-monocyte-derived macrophages (9). Burkitt's lymphoma Daudi (CCL-213, purchased in 2021) and myeloma U266 (TIB-196, purchased in 2019) cell lines were obtained from ATCC, tested for mycoplasma contamination by RT-qPCR, and cultured in RPMI 1640 medium supplemented with 10 % low-endotoxin FBS [< 0.5 endotoxin unit (EU) ml^{-1}], in the presence of penicillin/streptomycin (from now on termed as "culture medium"). All cell lines were used in passages 2–10. Neoplastic CD43^{-}B cells from MCL, DLBCL, FL2, NLPHL patients were isolated from lymph node suspensions by using the human B Cell Isolation Kit II (Miltenyi Biotec; > 98 % purity), as previously described (9). Neoplastic B cells were identified from their monoclonal expression of either the *k*- or the *l*-light chain by flow cytometry.

Flow cytometry analysis. Cocultured cells, including target cells (Daudi and U266 cell lines, neoplastic CD43^{-} B cells) and effector cells (freshly isolated NK cells or slan^{+}-monocytes) were resuspended in 50 µL of 1x PBS, 2 % FBS and 2 mM EDTA for antigen expression analysis and ADCP assays, or 15 mM EDTA for trogocytosis experiments (13). Cells were immediately incubated for 10 min at room T with 5 % human serum, and then stained for 30 min in ice using different panels of fluorochrome-conjugated mAbs (depending on the experiment type), including: CD45 BV510 (clone H130), CD16 PerCP-Cy5.5 (clone 3G8), CD38 APC-Cy7 (clone HIT2) from BioLegend; slan/MDC8 FITC (clone DD1), CD19 PE-VIO770 (clone LT19), CD56 PE (clone AF12-7H3), CD107a APC-Cy7 (clone REA792), CD47 APC (clone REA220) from Miltenyi Biotec. Phenotypic analysis was performed on live cells, identified by excluding either SytoxBlue^{+} or SytoxAAD^{+} dead cells. Sample fluorescence was measured by either 8-color MACSQuant10, or 14-color MACSQuant16, flow-cytometers (Miltenyi Biotec), while data analysis was performed by FlowJo software Version 10.1 (Tree Star Inc.). For CD19, CD38 and CD47 expression levels, their median fluorescence intensity (MFI) was compared to the MFI of the correspondent fluorescent minus one control (FMO). To detect intracellular TNFα, we used the FIX & PERM™ Cell Permeabilization Kit (Thermo-Fisher). Briefly, freshly isolated slan^{+}-monocytes were cocultured

for 1 h with Daudi cells (either uncoated or coated with 5 μg/mL RTX or 5F9/Magrolimab) at an E:T ratio of 10:1. Then, cocoltures were treated with 2 μg/mL Brefeldin A (BFA, InvivoGen) and incubated for 3 more h. Cells were then prepared for flow cytometry analysis and stained by slan/MDC8 FITC (Miltenyi Biotec) and (to exclude dead cells) Viobility 405/452 Fixable Dye (Miltenyi Biotec). Cocoltures were then fixed and permeabilized to detect intracellular TNFα by anti-human TNFα APC mAbs (clone MAb11 from Biolegend).

ADCC and phagocytosis assays. ADCC of Daudi or U266 cell lines was evaluated by the Calcein-Acetyoxymethyl (Calcein AM, Molecular Probes) cytotoxicity assay, as previously reported (9). Briefly, Daudi or U266 cell lines were initially stained with 10 μMol Calcein AM in 1x PBS plus 2 % FBS for 15 min at 37°. Cells were then adjusted to $1*10^6$/mL in culture medium and either left untreated or incubated for 20 min at 37° with: 0.5-10 μg/mL Rituximab (MABTHERA from Roche), and/or 0.5-10 μg/mL Hu5F9-G4/Magrolimab (kindly provided by M.P.C), depending on what specifically indicated in the results, or 5 μg/mL anti-CD38 (Daratumumab from Selleck Chemicals), 1-10 μg/mL anti-hCD20 IgG4 (InvivoGen), 10 μg/mL anti-CD47 B6H12 (ThermoFisher), 1-10 μg/mL anti-hCD47 IgG1 (BPS Bioscience). Then, $5*10^3$ target cells were transferred into U-bottom 96-well plates and cocultured with $5*10^4$ of freshly isolated NK cells or $slan^+$-monocytes (at an E:T ratio of 10:1) in a final volume of 150 μl. After 1-4 h of incubation, plate(s) were centrifuged and 50 μL of cell-free supernatants from each well were transferred, in duplicate, into a flat-bottom 96-well plates (Corning) and sample fluorescence was measured by a $VICTOR^3$ multilabel reader (PerkinElmer). Percent of specific lysis was calculated according to the formula: [(test release - spontaneous release)/(maximum release - spontaneous release)] x 100. Spontaneous and maximum release represent, respectively, Calcein AM release from target cells in medium alone or in medium plus 1 % Triton X-100 (9). In selected experiments, before coculture with target cells, effector cells were pre-treated at 37° for 1 h for with 100 nMol Concanamycin A (Sigma-Aldrich), or for 30 min with selected inhibitors, including: 10 μg/mL αFas mAbs (clone ZB4 from Sigma-Aldrich), 100 ng/mL sTRAILR (R&D), 500 μMol aNO L-NAME (Santa Cruz), 10 μg/mL Certolizumab (CIMZIA, kindly provided by C.T.), 50 μg/mL SOD (Merck, Sigma-Aldrich), 5 μg/mL Citochalasin B (Sigma-Aldrich), 5 μg/mL Citochalasin D (Sigma-Aldrich), 10 μg/mL $F(ab')_2$ anti-CD16 (Ancell). Conversely, target cells were pre-treated with 10 ug/mL Z-VAD-FMK (InvivoGen) or 10 μMoL NEC-1 (Santa Cruz) before coculture with effector cells, in other experiments. Phagocytosis experiments were done exactly as previously described (9).

Trogocytosis assay. Daudi, U266 or neoplastic B cells were initially stained with the PKH26 Red Fluorescent Cell Linker Midi Kit for General Cell Membrane Labelling (Sigma-Aldrich), according to the manufacturer's instructions (9). Then, cells were adjusted to $1*10^6$/mL and either left untreated, or incubated for 20 min at 37º with 5 μg/mL Rituximab, 5 μg/mL Hu5F9-G4/Magrolimab or 5 μg/mL anti-CD38/Daratumumab. PKH26-labeled target cells were then cocultured with freshly isolated NK cells or slan$^+$-monocytes under the same conditions described for the Calcein AM release assay. After 1-4 h of incubation, plates were centrifuged and pelleted cells prepared for the flow cytometry staining. In some experiments, before coculture, effector or target cells were pre-treated for 30 min at 37° with the inhibitors listed in the ADCC section.

Evaluation of trogocytosis by fluorescence and confocal microscopy. For experiments by fluorescence microscopy, Daudi cells were labeled using the MemBrite Fix 640/660 Cell Surface Staining Kit (Biotium), while slan$^+$-monocytes were labelled with 1 μMol Calcein AM dye. Then, $1*10^5$ effector cells and $1*10^4$ target cells (10:1 E:T ratio) were cocultured in a U-bottom 96-well plates, in a final volume of 150 μL. After 1 or 4 h, cells were collected and cytospins prepared for immunofluorescence microscopy analysis. Cells were centrifuged on Polysine Adhesion slides (Thermo Fisher), then fixed using 4 % paraformaldehyde in 1x PBS for 20 min at room T. After fixation, cells were washed with 1x PBS and permeabilized using 1x PBS containing 0.1 % Triton X-100 for 10 min at room T. Cells were then stained by DAPI to label the cell nuclei. High resolution images were acquired by a AxioImager.Z2 microscope equipped with Zen blue software at 63× magnification (Plan-Apochromat 63×/1.40 Oil DIC M27 objective lens) using Hamamatsu camera (Zeiss, Germany). Data are expressed as fluorescent area for both DAPI (nuclei marker) and Calcein AM dye (cytoplasm marker). Images were analyzed using Imaris software 9.6 (Oxford Instruments), adjusting brightness and contrast over the whole image by utilizing a Gaussian filter (0.103 μm). For confocal microscopy experiments, slan$^+$-monocytes and Calcein AM-labeled Daudi cells were collected from the same cocultures for ADCC assays and cytospins prepared as described above. In addition, after fixation, slan$^+$-monocytes were labeled by non-fluorescent anti-MDC8 IgM antibodies followed by APC anti-IgM secondary antibodies. Images were acquired by confocal laser scanning microscopy (LSM 510, Zeiss) (9).

Time-lapse microscopy. For live imaging studies, slan$^+$-monocytes were resuspended in Hank's buffer, while target cells (Daudi cells) were initially stained with 1 μMol Calcein AM and right after with PKH26 dye (as described above). Double-stained target cells were then incubated for 20 min at 37° with 5 μg/mL Rituximab, 5 μg/mL Hu5F9-G4/Magrolimab or 5 μg/mL Daratumumab,

and then resuspended in Hank's buffer. $1*10^5$ effector cells and $1*10^4$ target cells (10:1 E:T ratio) were cocultured in 96 flat-well plates in a final volume of 100 µL. 0.5 µM TO-PRO™-3 Iodide DNA binding dye (ThermoFisher) was also added to the coculture medium to assess cell viability (14). Live imaging acquisition started after 5-10 min of cell coculture by using a LD Plan-Neofluar 40×/0.6 Korr M27 objective lens assembled on the Axio Observer.Z1/7 microscope, equipped with a Hamamatsu camera and a thermostatic chamber (37°C, 5% CO2) (Zeiss, Germany). Exposure time was automatically set and left unchanged for the entire duration of the experiment. Time-lapse was acquired for 4 h under controlled conditions. Brightness and contrast were adjusted over the whole time-lapse duration with Imaris software 9.6 (Oxford Instruments).

Immunohistochemistry and digital analysis of tissues. FFPE tissue blocks were retrieved from the tissue bank of the Department of Pathology (Spedali Civili di Brescia, Brescia, Italy). Tissue analysis involved different lymphomas, including Burkitt lymphoma (BL, n=2), mantle cell lymphoma (MCL, n=1), double-hit diffuse large B cell lymphoma (DLBCL, n=1) and a case of DLBCL relapse after treatment with Rituximab (n=1). Four-micron thick tissue sections were used for double/triple immunohistochemical staining by antibodies from Leica Biosystems, including anti-CD19 (clone BT51E, diluted 1:40), anti-CD20 (clone L26, diluted 1:200) or anti-CD38 (clone SPC32, diluted 1:100). Antigens were revealed using Novolink Polymer followed by 3-amino-9-ethylcarbazole (AEC) chromogen. After completing the first immune reaction, anti-MDC8 antibody (from Miltenyi Biotec, clone DD1, diluted 1:120) was revealed after 40 min in EDTA-buffer pH 8.0 as antigen retrieval-using Mach4AP followed by Ferangi Blue. For triple staining, double stained slides were subjected to antigen retrieval, and then incubated with anti-PAX5 antibody (from BD, clone 24/PAX5, diluted 1:40) and visualized using Novolink polymer and 3,3'-diaminobenzidine (DAB) as chromogen. Omission of primary antibody as well as irrelevant antibody staining (anti Napsin from Leica Biosystems, clone IP64) were performed on two representative lymphoma samples as control staining. Samples were digitalized and optically analyzed with Aperio Scanscope CS. Images were taken as snapshot at 80X digital magnification.

Statistical analysis. Data are expressed as mean ± SEM. Depending on the experiment, statistical analysis between two groups were tested by two-tailed Student t test, while multiple comparisons were tested by one-way ANOVA followed by Tukey post-hoc test, or two-way ANOVA followed by Sidak post-hoc test. Evaluation of the percentages of ADCC inhibition in the presence of inhibitors was performed by using one sample t test. Statistical analysis was performed by Prism Version 9 software (GraphPad).

Study approval. Human samples were obtained following informed written consent. All experimental protocols were approved by the Ethic Committee of the Azienda Ospedaliera Integrata di Verona and Spedali Civili of Brescia (Italy). The methods were carried out in accordance with the approved guidelines. Retrospective analysis of archival material was conducted in compliance with the Declaration of Helsinki and with policies approved by the Ethics Board of Spedali Civili di Brescia.

RESULTS

slan$^+$-monocytes and NK cells exert ADCC *via* different effector mechanisms

Initial experiments using either blocking antibodies, or pharmacologic inhibitors, excluded that Fas ligand (FasL), TNF-related apoptosis-inducing ligand (TRAIL), nitric oxide (NO) or reactive oxygen species (ROS) function as cytotoxic mediators of RTX-dependent ADCC exerted by freshly isolated slan$^+$-monocytes and NK cells (**Supplementary Fig. S1A and S1B**). By contrast, concanamycin A (CMA), which is a specific inhibitor of lysosomal H^+-ATPase (the latter being necessary for perforin maturation) (15), was found to significantly reduce RTX-dependent ADCC by NK cells, but not slan$^+$-monocytes (**Supplementary Fig. S1A** and **S1B**).

We then explored whether Hu5F9-G4/Magrolimab (from hereafter 5F9/Magrolimab) could influence RTX-dependent ADCC, given their promising activity in patients with aggressive and indolent lymphoma when used in combination with RTX (16). 5F9/Magrolimab consist of humanized IgG4 antibodies designed to interfere with the recognition of CD47 by the SIRPα receptor, hence to remove a "don't eat me" signal used by cancer cells to escape cell clearance, for instance performed by macrophages (17,18). Control experiments confirmed that CD47 is expressed by our target cells (i.e., Daudi cells) (19), at higher levels than those expressed by slan$^+$-monocytes or NK cells (**Supplementary Fig. S1C**). Addition of increasing concentrations of 5F9/Magrolimab to RTX was found to increase the ADCC levels exerted by slan$^+$-monocytes (**Fig. 1A**), but not NK cells (**Fig. 1B**). However, simply by themselves, 5F9/Magrolimab were found to significantly promote ADCC by slan$^+$-monocytes, even more potently than RTX (**Fig. 1A** and **1B**). 5F9/Magrolimab-mediated ADCC by slan$^+$-monocytes was optimal at 5 μg/ml (**Supplementary Fig. S1D**), as well as additive with RTX when both antibodies were used at 0.5 μg/ml (**Supplementary Figure S1E**). In addition, 5F9/Magrolimab-mediated ADCC by slan$^+$-monocytes was almost completely prevented by anti-FcγRIIIA/CD16A $F(ab')_2$ antibodies (**Supplementary Fig. S1F**), which were also found to inhibit RTX-mediated ADCC by both slan$^+$-monocytes (**Supplementary Fig. S1F**) and NK cells (**Supplementary Fig. S1H**). Similarly to previous findings on monocyte-derived macrophages (17), 5F9/Magrolimab alone were also found to favor phagocytosis of Daudi cells by slan$^+$-macrophages generated *in vitro* (9), without however influencing the effect of RTX (**Supplementary Fig. S2A** and **S2B**). Notably, also other anti-CD47 antibodies, precisely murine (IgG1) B6H12 (20) were found to promote slan$^+$-monocyte-, but not NK cell-, mediated ADCC (**Fig. 1C**), confirming previous studies in the case of NK cells (17,19,21). Such an inability could be explained by the fact that NK cells very inefficiently bind either human IgG4 or murine IgG1 (22,23). Accordingly, even anti-CD20-hIgG4 antibodies did not trigger any NK cell-mediated ADCC in our hands (**Fig. 1D**), while they efficiently promoted ADCC

by slan$^+$-monocytes (**Fig. 1E**). Moreover, flow cytometry experiments uncovered that NK cells bind neither 5F9/Magrolimab nor B6H12 *via* FcγRIIIA/CD16A (**Supplementary Fig. S1I**). By contrast, anti-CD47-hIgG1 antibodies (hence matching the same IgG isotypes of RTX) were found to directly promote NK cell-mediated ADCC of Daudi cells (**Figure 1F**). These new results confirm that discrete IgG isotypes only allow NK cells to perform ADCC.

In a further series of experiments, we found that Certolizumab, a PEGylated Fab' fragment of a humanized mAb inhibiting TNFα (24), partially, but significantly, reduced either RTX-, or (at higher levels) 5F9/Magrolimab-, dependent ADCC by slan$^+$-monocytes, without however influencing that by NK cells (**Fig. 1G**). On the other hand, either Z-VAD-FMK (an irreversible inhibitor of apoptosis induction), or NEC-1 (an inhibitor of death domain receptor-associated adaptor kinase RIP1), were found not to affect ADCC by slan$^+$-monocytes (**Fig. 1H**), therefore ruling out an induction of, respectively, extrinsic apoptosis and caspase-independent necroptosis.

Taken together, these experiments demonstrated that slan$^+$-monocytes and NK cells exert ADCC of target cells through different mechanisms, namely: i) a non-apoptotic lytic type of cell death, putatively involving TNFα, undertaken by slan$^+$-monocytes; ii) a perforin-dependent, TNFα-independent, cytotoxicity by NK cells, as expected (25). These experiments also uncovered that slan$^+$-monocytes, but not NK cells, perform a 5F9/Magrolimab-dependent ADCC of target cells requiring FcγRIIIA/CD16A.

slan$^+$-monocytes perform trogocytosis of antibody-coated target cells

Subsequent experiments demonstrated that supernatants harvested from cocultures of slan$^+$-monocytes with target cells (coated or not with either RTX or 5F9/Magrolimab), and successively transferred to fresh target cells, do not alter the viability of the latter cells (**Supplementary Fig. S3A**). These results suggested that soluble mediator(s), likely released by slan$^+$-monocytes, are unable to directly trigger target cell death. Consistently, experiments by confocal microscopy demonstrated that, in the presence of RTX, slan$^+$-monocytes (i.e., MDC8$^+$cells in panels I and III of **Supplementary Fig. S3B and S3C**) engage interactions with Calcein AM-loaded target cells (i.e., green cells in panels I and II of **Supplementary Fig. S3B and S3C**). Moreover, as compared to those unbound, target cells bound to slan$^+$-monocytes were found to display a reduction in intracellular Calcein AM labeling (indicated by the arrows in panel II of **Supplementary Fig. S3B and S3C**), a change in the nuclear structure (indicated by the arrows in panels III of **Supplementary Fig. S3B and S3C**) and a destabilization of the membrane integrity/shape (indicated by the arrows in the brightfield plot in panel IV of **Supplementary Fig. S3B and S3C**). Consistently, quantification of the fluorescent area related to the intracellular Calcein AM dye

demonstrated significant reductions exclusively when RTX-coated Daudi cells are in direct contact with slan$^+$-monocytes, but not if unbound to them, or as compared to uncoated Daudi cells, bound or not to slan$^+$-monocytes (**Supplementary Fig. S3D)**. Similar results were obtained for DAPI staining of Daudi cell nuclei, which was found to significantly decrease in fluorescence under the same conditions described for the Calcein AM dye measurement (**Supplementary Fig. S3E)**. In other words, target cells bound to slan$^+$-monocytes were found to display features of dying cells, pointing toward the requirement of strict interactions between slan$^+$-monocytes and antibody-coated target cells to ultimately trigger the death of the latter ones. The findings shown in **Supplementary Fig. S3A-D**, together with the those on the non-involvement of soluble cytotoxic mediators or perforin in the slan$^+$-monocyte-mediated ADCC (**Supplementary Fig. S1A-B**), recalled analogous observations that led Matlung *et al*. (14) to discover that human neutrophils perform trogocytosis. This process occurs *via* cell-cell contact dependent mechanisms and may trigger an active, mechanic, disruption of target cell membranes that ultimately might lead to a lytic (i.e., necrotic) type of cell death renamed as trogoptosis (26). Thus, to investigate whether slan$^+$-monocytes perform trogocytosis too, we performed immunofluorescence microscopy experiments in which target cells and slan$^+$-monocytes were labelled with, respectively, MemBrite Fix Dye and Calcein AM (**Fig. 2A** and **2B**), thus allowing the visualization of membrane transfer. As expected from **Supplementary Fig. S3**, slan$^+$-monocytes (green cells in panels **II** and **V** of **Fig. 2A** and **2B**) were found to establish direct contacts with either RTX-coated (**Fig. 2A**) or 5F9/Magrolimab-coated (**Fig. 2B)** target cells (red cells). Noticeably, both merged images (panels **III** and **VI** of **Fig. 2A** and **2B**) and single MemBrite/red fluorescence (panels **I** and **IV** of **Fig. 2A** and **2B**), revealed dots of red fluorescence localized on slan$^+$-monocyte membranes (indicated by the arrows), suggesting that fragments of target cell membranes were physically extracted by slan$^+$-monocytes. In these experiments, nuclear staining with DAPI confirmed that none of the slan$^+$-monocytes contained more than one nucleus (**Fig. 2A** and **2B**), demonstrating that phagocytosis was neither the cause of the transferred membrane fragments, nor the cytotoxic mechanism.

All in all, these immunofluorescence microscopy experiments suggest that slan$^+$-monocytes, once attached to target cells, nibble fragments of their membranes, thus pointing for a trogocytic phenomenon.

Flow cytometry experiments confirm that slan$^+$-monocytes exert trogocytosis

In subsequent experiments, we aimed at further confirming, as well as quantifying, the capacity of slan$^+$-monocytes to exert trogocytosis. By flow cytometry, slan$^+$-monocytes (i.e., purple MDC8$^+$ cells in **Fig. 3A**) cocultured with PKH26-labelled target cells (i.e., red cells in left panels of

Fig. 3A) were found to become PKH26$^+$ as early as after 1 h in the presence of either RTX or 5F9/Magrolimab (i.e., PKH26$^+$MDC8$^+$cells in middle panels of **Fig. 3A**), as well as to greatly increase their PKH26 positivity after 4 h (**Fig. 3B**). slan$^+$-monocytes were also found to progressively downmodulate their FcγRIIIA/CD16A levels (histograms in right panels of both **Fig. 3A** and **3B**), likely as a result of antibody-mediated binding to CD16A, and similarly to what observed in the case of NK cells after RTX- (dotted arrow in right panel of **Supplementary Fig. S4A**), but not 5F9/Magrolimab-, dependent ADCC. Consistently, expression of CD107a/LAMP-1 (a degranulation marker) was found to increase in NK cells only upon RTX-dependent ADCC, in concomitance to Daudi cell death (**Supplementary Fig. S4A**). Moreover, by monitoring cell viability up to 4 h, we found that slan$^+$-monocyte-mediated trogocytosis ultimately leads to target cell death exclusively in the presence of either RTX or 5F9/Magrolimab. In fact, the increased percentage of PKH26$^+$MDC8$^+$-monocytes observed at 4 h (**Fig. 3B**) was found to coincide with a reduction of the number of PKH26-labelled target cells (red cells in left panels of **Fig. 3B**). Importantly, a concomitant quantification of both ADCC (**Fig. 3C**) and trogocytosis (**Fig. 3D**) demonstrated that the killing of target cells by slan$^+$-monocytes always occurs after the initiation of the trogocytic events.

Since the "shaving" by effector cells of membrane molecules from the target cells, concomitantly with their acquisition, represents one of the hallmarks of trogocytosis (27), we then investigated whether slan$^+$-monocytes trim CD19 and CD38 from target cells and acquire them. Flow cytometry experiments confirmed so (**Fig. 3E**), in concomitance with a decrease of CD19 and CD38 expression by target cells (**Fig. 3F**). Furthermore, two cytoskeleton inhibitors acting *via* different mechanisms (28), namely cytochalasin B and cytochalasin D, were found to suppress both slan$^+$-monocyte-mediated trogocytosis (Supplementary Fig. S4B) and slan$^+$-monocyte-mediated ADCC (Supplementary Fig. S4C), thus linking the two processes. In these groups of experiments, Certolizumab was found to significantly inhibit antibody-dependent trogocytosis of target cells by slan$^+$-monocytes after 4, but not 1, h of coculture (**Fig. 4A** and **4B**), thus only in coincidence with ADCC (**Fig. 1F**). Certolizumab was also found to inhibit FcγRIIIA/CD16A downmodulation by slan$^+$-monocytes (see **Fig. 3A** and **3B**), again after 4 h (**Fig. 4B**), but not 1 h (data not shown), of coculture. Notably, only slan$^+$-monocytes were found to express intracellular TNFα when cocultured with either RTX or 5F9/Magrolimab Daudi cells (**Fig. 4C**), thus demonstrating that they represent the sole TNFα-producing cells. Finally, flow cytometry experiments confirmed (29) that also NK cells perform trogocytosis in the presence of RTX-coated Daudi cells (but not 5F9/Magrolimab) (**Supplementary Fig. S4D**), however at lower levels than those by slan$^+$-monocytes. Moreover, NK cells were found to perform maximal trogocytosis already after 1 h

(**Supplementary Fig. S4D**), without increasing it at 4 h (as in the case of slan$^+$-monocytes), and thus not matching their ADCC kinetics (**Supplementary Fig. S4E**).

In summary, data from flow cytometry experiments detecting the capture of target membrane fragments and antigens, combined with those from the effects exerted by cytoskeletal inhibitors, further strengthened the findings that slan$^+$-monocytes perform trogocytosis. The latter process is sustained by endogenous TNFα and is causally related to the death of antibody-coated target cells.

slan$^+$-monocytes kill cancer cells by trogoptosis

Then, we investigated the correlation between antibody-mediated trogocytosis and target cell death by live cell imaging of slan$^+$-monocytes cocultured with RTX-/Magrolimab-coated target cells. As shown in **Supplementary Videos** 1 and 2, as well as selected frames in **Fig. 5A** and **5B**, slan$^+$-monocytes were found to display a very active and motile behavior, distinguished by transient, but repetitive, cell-cell contacts with antibody-coated target cells, likely dependent on the binding to either RTX (**Supplementary Video** 1) or 5F9/Magrolimab (**Supplementary Video** 2). Some of these contacts were found to promote swelling and bleb formation of target cell membranes (**Supplementary Videos** 1 and 2, and green boxes **Fig. 5A** and **5B**). Cell-cell contacts were found to become tighter over time, with slan$^+$-monocytes surrounding and nibbling off target cell membranes (**Supplementary Videos** 1 and 2, and red boxes in **Fig. 5A** and **5B**). At the latter stage, loss of plasma membrane integrity, rapid reduction of cytoplasmic labelling due to membrane rupture/permeabilization and, ultimately, death of target cells could be observed (**Supplementary Videos** 1 and 2, and blue boxes in **Fig. 5A** and **5B**).

All in all, live cell imaging unequivocally demonstrated that the antibody-mediated trogocytic process exerted by slan$^+$-monocytes ultimately ends into target cell death, likely into trogoptosis.

slan$^+$-monocytes mediate Daratumumab-dependent trogoptosis

We then explored whether slan$^+$-monocytes promote antibody-mediated ADCC also *via* Daratumumab (DARA). The latter are human IgG1 antibodies recognizing CD38, an antigen expressed at high levels in multiple myeloma (MM) cells (30), as well as in malignant lymphoid cells of patients with DLBCL, mantle cell lymphoma (MCL) or B cell chronic lymphocytic leukemia (B-CLL) (31). Noticeably, a very bright CD38 expression by lymphoma cells appears to correlate with an adverse prognosis (31). DARA also represent the first-in-class human-specific anti-CD38 mAbs approved for the treatment of MM patients (30), and known to promote NK cell-

mediated ADCC (32). In this context, we found that slan$^+$-monocytes perform an efficient ADCC of both Daudi (**Fig. 6A**) and U266 myeloma (**Fig. 6B**) cells in the presence of DARA. By flow cytometry (**Fig. 6C**) and immunofluorescence microscopy (**Fig. 6D**) experiments, we also found that slan$^+$-monocytes perform a DARA-mediated trogocytosis of target cells. DARA-mediated ADCC was found not influenced by SOD (a ROS inhibitor) (**Fig. 6E**), while both DARA-mediated ADCC and trogocytosis were TNFα-independent (**Fig. 6F, 6G**), as observed for RTX. Moreover, live cell imaging (**Supplementary Video 3** and **Fig. 6H**) ultimately demonstrated that slan$^+$-monocytes kill DARA-coated Daudi cells by trogoptosis, substantially recapitulating our previous observations using RTX or 5F9/Magrolimab.

slan$^+$-monocyte mediated-trogocytosis of neoplastic B cells from lymphoma patients

In final experiments we found that slan$^+$-monocytes, in the presence of either RTX or 5F9/Magrolimab, perform trogocytosis of neoplastic B cells isolated from neoplastic tissues of patients affected by various lymphoma types (9), including DLBCL, MCL and FL (**Fig. 7A-D**). These results were obtained by flow cytometry investigating either trogocytosis of lymphoma cells (**Fig. 7A-C**), or CD19 and CD38 acquisition (**Fig. 7D**). Under these experimental settings, RTX appeared to be more effective than 5F9/Magrolimab (**Fig. 7C**). Moreover, by immunohistochemistry, we could detect indirect evidence of endogenous trogocytosis of neoplastic B cells by slan$^+$-cells in different types of B cell lymphoma samples (**Fig. 7E**). More specifically, by either double or triple immunostaining using MDC8 antibody to stain slan$^+$-cells, we could detect partial (or punctate) co-expression of CD19, CD20 (arrows in **Fig. 7E**) and CD38 (inset in panel I of **Fig. 7E**) on the cell membranes of MDC8$^+$-cells in Burkitt lymphoma (BL, arrows in panels I and II of **Fig. 7E**), double hit lymphoma DLBCL (DHL, arrows in panel III of **Fig. 7E**), MCL (arrows in panel IV of **Fig. 7E**), and a case of DLBCL relapse after Rituximab treatment (arrows in panels V-VI of **Fig. 7E**). In these experiments, Pax5 nuclear reactivity allowed an unequivocal identification of lymphoma cells (panels VII of **Fig. 7E**). On the other hand, linear or punctate staining on the membrane of MDC8$^+$-cells was completely lacking on negative control stain for CD19 (Supplementary Fig. S5), CD20 and CD38 (data not shown) Altogether, these data suggest that, very likely, spontaneous antibodies towards surface receptors of lymphoma cells are produced, and that lymphoma-associated slan$^+$-cells likely mediate endogenous trogocytosis of neoplastic B cells.

DISCUSSION

Data from this study indicate that slan$^+$-monocytes and NK cells utilize different effector mechanisms for ADCC. In fact, while we excluded the involvement of FasL, TRAIL and [as previously reported (33)] ROS or NO as mediators for RTX-dependent ADCC of neoplastic B cells by both slan$^+$-monocytes and NK cells, perforin was ruled out only for RTX-dependent ADCC by slan$^+$-monocytes. Diverse results between slan$^+$-monocytes and NK cells were also obtained by examining the effect of 5F9/Magrolimab on RTX-dependent ADCC. 5F9/Magrolimab are humanized IgG4 anti-CD47 antibodies designed to interfere with the recognition of CD47 by the SIRPα receptor, hence to remove a "don't eat me" signal used by cancer cells to escape cell clearance by phagocytes (18). Among the variety of therapeutic anti-CD47 antibodies to date developed, 5F9/Magrolimab are among the most clinically advanced CD47-targeting agent used for a series of hematologic and solid neoplasms (18,34)(Clinicaltrials.gov Identifier: NCT04827576, NCT05627466, NCT04313881). Specifically, 5F9/Magrolimab are typically used in combination with other therapeutic antibodies and/or pharmacological agents for hematologic cancers including myelodysplastic syndrome (MDS), acute myeloid leukemia (AML) and relapsed/refractory B-cell non-Hodgkin lymphoma (NHL) (18). Moreover, 5F9/Magrolimab are used in combination with Rituximab in refractory NHL, with a promising efficacy and tolerability (16)(Clinicaltrials.gov Identifier: NCT02953509). In our *in vitro* experiments, 5F9/Magrolimab did not significantly increase the RTX-mediated ADCC by both slan$^+$-monocytes and NK cells, as well as the ADPC of Daudi cells by slan$^+$-macrophages. On the other hand, 5F9/Magrolimab alone were found to directly promote ADCC by slan$^+$-monocytes, but not by NK cells, as well as cancer cell phagocytosis by slan$^+$-macrophages, in the latter case similarly to monocyte-derived macrophages (17). Moreover, not only other anti-CD47 antibodies such as B6H12 (20), but even anti-CD20-hIgG4 antibodies were found unable to promote ADCC of target cells by NK cells. Since ADCC by both slan$^+$-monocytes and NK cells depends on the involvement FcγRIIIA/CD16A, we speculated that the inability to perform 5F9/Magrolimab-mediated ADCC by NK cells could derive from the poor affinity of their FcγRIIIA/CD16A for the IgG4 subclass (23). Indeed, NK cells and non-classical monocytes/slan$^+$-monocytes express FcγRIIIA/CD16A with different properties, as revealed by a glycoproteomic characterization of their purified FcγRIIIA/CD16A molecules revealing differences in the glycosylation of several regions (35,36). Moreover, N-Acetyllactosamine (LacNAc) repeats have been consistently detected in several N-glycan sites of FcγRIIIA/CD16A present in non-classical monocytes (35). In this context, experiments done to revise the manuscript demonstrated that anti-CD47-hIgG1 antibodies can directly promote ADCC by NK cells. All in all, our data ultimately confirm that 5F9/Magrolimab does not directly trigger ADCC by NK cells since its

hIgG4-containing fragment does not bind to FcγRIIIA/CD16A as instead likely done by the hIgG1 portion of the anti-CD47-hIgG1 antibodies. In any case, our observations that 5F9/Magrolimab alone directly promote both tumor cell phagocytosis by slan$^+$-macrophages and ADCC by slan$^+$-monocytes, but not by NK cells, are clinically remarkable for their potential contribution to the eradication of tumor cells, as observed in AML (Clinicaltrials.gov Identifier NCT04778397), MDS (Clinicaltrials.gov Identifier NCT04313881) and NHL (Clinicaltrials.gov Identifier NCT02953509) patients. The involvement of slan$^+$-monocyte-mediated trogoptosis, in fact, might contribute to amplify the anti-cancer effect of 5F9/Magrolimab when these antibodies are associated to other therapeutic agents.

Confocal microscopy experiments demonstrated that slan$^+$-monocytes engage direct interactions with RTX-covered target cells, similarly to neutrophils cocultured with anti-HER2-coated SKBR3 breast cancer cells that ultimately were shown to perform trogocytosis (14). The latter is a process of cell-cell interaction during which an effector cell nibbles, and then rapidly ingests, membrane fragments of a target cell. Among various consequences of trogocytosis (26,27), trogoptosis represents a form of trogocytosis-related process characterized by a lytic (i.e., necrotic) type of cell death, for example exerted by neutrophils (14,37). Immunofluorescence microscopy experiments uncovered that also slan$^+$-monocytes perform, as early as after 1 h, either RTX- or 5F9/Magrolimab-dependent trogocytosis. As shown by flow cytometry-based analysis, slan$^+$-monocytes acquire membrane fragments of PKH26-labeled target cells already within 1 h in the presence of either RTX or 5F9/Magrolimab, further increasing membrane transfer up to 4 h, in concomitance with target cell death, thus matching ADCC kinetics. Not surprisingly, slan$^+$-monocytes were found to acquire CD19 and CD38 antigens from target cell membranes, a well-known phenomenon consequent to trogocytosis named as “shaving effect”. Consistent with these novel set of *in vitro* findings, our microscopic studies of human biopsies displaying slan$^+$-cells closely interacting with lymphoma cells (9) provide evidence for an endogenous shaving of neoplastic B cells by slan$^+$-cells, not only in a case of DLBCL relapse after Rituximab treatment, but also in untreated BL, MCL, DHL patients. We would thus speculate that, in the latter patients, spontaneous antibodies towards surface receptors of lymphoma cells are produced and engage slan$^+$-cells. Finally, we could additionally show that, in the presence of either RTX or 5F9/Magrolimab, peripheral slan$^+$-monocytes perform trogocytosis of neoplastic B cells from various lymphoma types, including DLBCL, MCL and FL. Collectively, our data prove that slan$^+$-monocytes, as well as their tissue counterparts, efficiently perform trogocytosis of target cells. In addition, live cell imaging demonstrated that slan$^+$-monocytes perform repeated trogocytic attacks of either RTX- or Magrolimab-coated target cells, which ultimately undergo cell death due to loss

of plasma membrane integrity. Similarly to what described for neutrophils (14), or for the amoeba *Naegleria fowleri* (27,38), these findings resembled the process of trogoptosis.

Notably, trogocytosis and ADCC of target cells by slan$^+$-monocytes partially require endogenous TNFα, especially in the presence of 5F9/Magrolimab. These observations are consistent with previous studies pointing a role for TNFα in the ADCC of either 17-1A-coated COLO 205 cell line by slan$^+$-monocytes (39) or of KM966-coated A549 cell line by non-classical monocytes (33). However, they are in contrast with concomitant data excluding that soluble mediators derived from slan$^+$-monocyte/Daudi cell cocultures could directly kill target cells, or that RTX- or 5F9/Magrolimab-mediated ADCC relies on a TNFα-dependent apoptosis/necroptosis phenomenon. These contrasting findings were reconciled by experiments from this study demonstrating that endogenous TNFα sustains trogocytosis once it is already initiated. How endogenous TNFα maintains an ongoing trogocytosis remains, however, to be investigated. It is possible that endogenous TNFα may autocrinally activate slan$^+$-monocytes, thus potentiating their cytotoxic effects. Accordingly, incubation of Daudi cells for 4 h with 100 and 1000 ng/mL of recombinant TNFα was found not to affect their viability. We also found that slan$^+$-monocytes perform an efficient Daratumumab-mediated trogocytosis and trogoptosis/ADCC of target cells, an observation that not only extends the cytotoxic potential by slan$^+$-monocytes *via* additional therapeutic antibodies, but that also has important implications for MM patients. In fact, a reduction of Daratumumab-mediated NK-cell ADCC has been observed in MM patients (40), explained as a Daratumumab-induced fratricide NK cytotoxicity phenomenon (41,42) due to high levels of CD38 by NK cells (43). However, the remaining PBMC fractions of the same patients maintain the ability to carry out an *ex vivo* Daratumumab-mediated ADCC (40), thus pointing for other ADCC effector cells. Since a rapid trogocytosis-dependent shaving of CD38 from MM cells by myeloid cells was described following Daratumumab infusion (44), we propose a role for slan$^+$-monocytes under this therapeutic setting. It is worth mentioning that our experiments also confirmed (29) that NK cells perform trogocytosis of RTX- (but not 5F9/Magrolimab)-coated Daudi cells. However, supporting previous data (14), our observations also indicate that trogocytosis by NK cells does not directly induce target cell death via trogoptosis, differently from that by slan$^+$-monocytes.

In conclusion, this work uncovers that slan$^+$-monocytes kill tumor cells *via* trogoptosis. Several targeted agents and approaches are being developed to enhance the immune system to more efficiently eliminate cancer cells (45,46), including the infusion of compatible NK cells (47), the generation of mAbs with higher binding capacity to the target antigen (48), and the glycoengineering the Fc N-glycan region of antibodies to increase affinity to CD16 (49). Based on our findings, it would be reasonable to exploit slan$^+$-monocyte-mediated trogoptosis as a novel

weapon to kill cancer cells, especially when NK cells are ineffective. Moreover, even though induction of phagocytosis/promotion of “eat me” signaling to macrophages is supposed to be the cytotoxic mechanism whereby 5F9/Magrolimab function in cancer patients (50), our data suggest that ADCC mediated by slan^{+}-monocytes could represent an unsuspected 5F9/Magrolimab-triggered effect, which must be carefully investigated *in vivo*.

Authors' contributions

G.F.: Conceptualization, data curation, formal analysis, validation, methodology, writing original draft. **E.P.:** methodology, data curation, formal analysis and editing. **C.B.:** validation. **S.L**.: validation, methodology. **C.T.**: providing material, writing, and editing. **G.C.**: writing and editing. **M.P.C.:** providing material. **W.V.:** providing material, writing and editing. **M.A.C**.: project administration, resources, supervision, funding acquisition, writing review and editing.

Acknowledgments

We thank Stefania Zini (supported by Fondazione Beretta) and Mattia Bugatti for excellent technical support.

Abbreviation list

ADCP	Antibody-dependent cellular phagocytosis
AML	Acute myeloid leukemia
B-CLL	B cell chronic lymphocytic leukemia
BL	Burkitt lymphoma
Calcein AM	Calcein-Acetoxymethyl
CMA	Concanamycin A
DARA	Daratumumab/anti-CD38 monoclonal antibodies
DLBCL	Diffuse large B cell lymphoma
DHL	Double hit lymphoma DLBCLs
FFPE	Formalin Fixed Paraffin Embedded
FasL	Fas ligand
LAMP-1/CD107a	Lysosomal Associated Membrane protein 1
5F9/Magrolimab	Hu5F9-G4/Magrolimab/anti-CD47 monoclonal antibodies
MCL	Mantle cell lymphoma
MDS	Myelodysplastic syndrome
MM	Multiple myeloma
NHL	Non-Hodgkin lymphoma
NEC-1	Necrostatin-1
αNO L-NAME	NG-Nitro-L-arginine methyl ester hydrochloride
PKH26	PKH26 Red Fluorescent Cell Linker Midi Kit
RTX	Rituximab/anti-CD20 monoclonal antibodies
ROS	Reactive oxygen species
slan	6-sulfo LacNac (N-Acetyllactosamine)
slanDC	$slan^{+}$-dendritic cell
SIRPα	Signal regulatory protein alpha
TRAIL	TNF-related apoptosis-inducing ligand
TRAILR	TNF-related apoptosis-inducing ligand receptor
Z-VAD-FMK	N-Benzyloxycarbonyl-Val-Ala-Asp(O-Me) fluoromethyl ketone

REFERENCES

1. Ziegler-Heitbrock L, Ancuta P, Crowe S, Dalod M, Grau V, Hart DN, *et al.* Nomenclature of monocytes and dendritic cells in blood. Blood **2010**;116(16):e74-80 doi 10.1182/blood-2010-02-258558.
2. Ziegler-Heitbrock L, Hofer TP. Toward a refined definition of monocyte subsets. Front Immunol **2013**;4:23 doi 10.3389/fimmu.2013.00023.
3. Ozanska A, Szymczak D, Rybka J. Pattern of human monocyte subpopulations in health and disease. Scand J Immunol **2020**;92(1):e12883 doi 10.1111/sji.12883.
4. Schakel K, Kannagi R, Kniep B, Goto Y, Mitsuoka C, Zwirner J, *et al.* 6-Sulfo LacNAc, a novel carbohydrate modification of PSGL-1, defines an inflammatory type of human dendritic cells. Immunity **2002**;17(3):289-301 doi 10.1016/s1074-7613(02)00393-x.
5. Hofer TP, Zawada AM, Frankenberger M, Skokann K, Satzl AA, Gesierich W, *et al.* slan-defined subsets of CD16-positive monocytes: impact of granulomatous inflammation and M-CSF receptor mutation. Blood **2015**;126(24):2601-10 doi 10.1182/blood-2015-06-651331.
6. Hofer TP, van de Loosdrecht AA, Stahl-Hennig C, Cassatella MA, Ziegler-Heitbrock L. 6-Sulfo LacNAc (Slan) as a Marker for Non-classical Monocytes. Front Immunol **2019**;10:2052 doi 10.3389/fimmu.2019.02052.
7. Ahmad F, Dobel T, Schmitz M, Schakel K. Current Concepts on 6-sulfo LacNAc Expressing Monocytes (slanMo). Front Immunol **2019**;10:948 doi 10.3389/fimmu.2019.00948.
8. Vermi W, Micheletti A, Lonardi S, Costantini C, Calzetti F, Nascimbeni R, *et al.* slanDCs selectively accumulate in carcinoma-draining lymph nodes and marginate metastatic cells. Nat Commun **2014**;5:3029 doi 10.1038/ncomms4029.
9. Vermi W, Micheletti A, Finotti G, Tecchio C, Calzetti F, Costa S, *et al.* slan(+) Monocytes and Macrophages Mediate CD20-Dependent B-cell Lymphoma Elimination via ADCC and ADCP. Cancer Res **2018**;78(13):3544-59 doi 10.1158/0008-5472.CAN-17-2344.
10. Ng WL, Ansell SM, Mondello P. Insights into the tumor microenvironment of B cell lymphoma. J Exp Clin Cancer Res **2022**;41(1):362 doi 10.1186/s13046-022-02579-9.
11. Tamma R, Ranieri G, Ingravallo G, Annese T, Oranger A, Gaudio F, *et al.* Inflammatory Cells in Diffuse Large B Cell Lymphoma. J Clin Med **2020**;9(8) doi 10.3390/jcm9082418.
12. Plonquet A, Haioun C, Jais JP, Debard AL, Salles G, Bene MC, *et al.* Peripheral blood natural killer cell count is associated with clinical outcome in patients with aaIPI 2-3 diffuse large B-cell lymphoma. Ann Oncol **2007**;18(7):1209-15 doi 10.1093/annonc/mdm110.
13. Richardson SI, Crowther C, Mkhize NN, Morris L. Measuring the ability of HIV-specific antibodies to mediate trogocytosis. J Immunol Methods **2018**;463:71-83 doi 10.1016/j.jim.2018.09.009.
14. Matlung HL, Babes L, Zhao XW, van Houdt M, Treffers LW, van Rees DJ, *et al.* Neutrophils Kill Antibody-Opsonized Cancer Cells by Trogoptosis. Cell Rep **2018**;23(13):3946-59 e6 doi 10.1016/j.celrep.2018.05.082.
15. Kataoka T, Shinohara N, Takayama H, Takaku K, Kondo S, Yonehara S, *et al.* Concanamycin A, a powerful tool for characterization and estimation of contribution of perforin- and Fas-based lytic pathways in cell-mediated cytotoxicity. J Immunol **1996**;156(10):3678-86.
16. Advani R, Flinn I, Popplewell L, Forero A, Bartlett NL, Ghosh N, *et al.* CD47 Blockade by Hu5F9-G4 and Rituximab in Non-Hodgkin's Lymphoma. N Engl J Med **2018**;379(18):1711-21 doi 10.1056/NEJMoa1807315.
17. Liu J, Wang L, Zhao F, Tseng S, Narayanan C, Shura L, *et al.* Pre-Clinical Development of a Humanized Anti-CD47 Antibody with Anti-Cancer Therapeutic Potential. PLoS One **2015**;10(9):e0137345 doi 10.1371/journal.pone.0137345.

18. Maute R, Xu J, Weissman IL. CD47-SIRPalpha-targeted therapeutics: status and prospects. Immunooncol Technol **2022**;13:100070 doi 10.1016/j.iotech.2022.100070.
19. Jain S, Van Scoyk A, Morgan EA, Matthews A, Stevenson K, Newton G, *et al.* Targeted inhibition of CD47-SIRPalpha requires Fc-FcgammaR interactions to maximize activity in T-cell lymphomas. Blood **2019**;134(17):1430-40 doi 10.1182/blood.2019001744.
20. Pietsch EC, Dong J, Cardoso R, Zhang X, Chin D, Hawkins R, *et al.* Anti-leukemic activity and tolerability of anti-human CD47 monoclonal antibodies. Blood Cancer J **2017**;7(2):e536 doi 10.1038/bcj.2017.7.
21. Chao MP, Alizadeh AA, Tang C, Myklebust JH, Varghese B, Gill S, *et al.* Anti-CD47 antibody synergizes with rituximab to promote phagocytosis and eradicate non-Hodgkin lymphoma. Cell **2010**;142(5):699-713 doi 10.1016/j.cell.2010.07.044.
22. Clemenceau B, Vivien R, Pellat C, Foss M, Thibault G, Vie H. The human natural killer cytotoxic cell line NK-92, once armed with a murine CD16 receptor, represents a convenient cellular tool for the screening of mouse mAbs according to their ADCC potential. MAbs **2013**;5(4):587-94 doi 10.4161/mabs.25077.
23. Freitas Monteiro M, Papaserafeim M, Real A, Puga Yung GL, Seebach JD. Anti-CD20 rituximab IgG1, IgG3, and IgG4 but not IgG2 subclass trigger Ca(2+) mobilization and cytotoxicity in human NK cells. J Leukoc Biol **2020**;108(4):1409-23 doi 10.1002/JLB.5MA0620-039R.
24. Nesbitt A, Fossati G, Bergin M, Stephens P, Stephens S, Foulkes R, *et al.* Mechanism of action of certolizumab pegol (CDP870): in vitro comparison with other anti-tumor necrosis factor alpha agents. Inflamm Bowel Dis **2007**;13(11):1323-32 doi 10.1002/ibd.20225.
25. Anft M, Netter P, Urlaub D, Prager I, Schaffner S, Watzl C. NK cell detachment from target cells is regulated by successful cytotoxicity and influences cytokine production. Cell Mol Immunol **2020**;17(4):347-55 doi 10.1038/s41423-019-0277-2.
26. Miyake K, Karasuyama H. The Role of Trogocytosis in the Modulation of Immune Cell Functions. Cells **2021**;10(5) doi 10.3390/cells10051255.
27. Bettadapur A, Miller HW, Ralston KS. Biting Off What Can Be Chewed: Trogocytosis in Health, Infection, and Disease. Infect Immun **2020**;88(7) doi 10.1128/IAI.00930-19.
28. Trendowski M. Using cytochalasins to improve current chemotherapeutic approaches. Anticancer Agents Med Chem **2015**;15(3):327-35 doi 10.2174/1871520614666141016164335.
29. Hasim MS, Marotel M, Hodgins JJ, Vulpis E, Makinson OJ, Asif S, *et al.* When killers become thieves: Trogocytosed PD-1 inhibits NK cells in cancer. Sci Adv **2022**;8(15):eabj3286 doi 10.1126/sciadv.abj3286.
30. Sanchez L, Wang Y, Siegel DS, Wang ML. Daratumumab: a first-in-class CD38 monoclonal antibody for the treatment of multiple myeloma. J Hematol Oncol **2016**;9(1):51 doi 10.1186/s13045-016-0283-0.
31. Calabretta E, Carlo-Stella C. The Many Facets of CD38 in Lymphoma: From Tumor-Microenvironment Cell Interactions to Acquired Resistance to Immunotherapy. Cells **2020**;9(4) doi 10.3390/cells9040802.
32. Nijhof IS, Lammerts van Bueren JJ, van Kessel B, Andre P, Morel Y, Lokhorst HM, *et al.* Daratumumab-mediated lysis of primary multiple myeloma cells is enhanced in combination with the human anti-KIR antibody IPH2102 and lenalidomide. Haematologica **2015**;100(2):263-8 doi 10.3324/haematol.2014.117531.
33. Yeap WH, Wong KL, Shimasaki N, Teo EC, Quek JK, Yong HX, *et al.* CD16 is indispensable for antibody-dependent cellular cytotoxicity by human monocytes. Sci Rep **2016**;6:34310 doi 10.1038/srep34310.
34. Jalil AR, Andrechak JC, Discher DE. Macrophage checkpoint blockade: results from initial clinical trials, binding analyses, and CD47-SIRPalpha structure-function. Antib Ther **2020**;3(2):80-94 doi 10.1093/abt/tbaa006.

35. Roberts JT, Patel KR, Barb AW. Site-specific N-glycan Analysis of Antibody-binding Fc gamma Receptors from Primary Human Monocytes. Mol Cell Proteomics **2020**;19(2):362-74 doi 10.1074/mcp.RA119.001733.
36. Barb AW. Fc gamma receptor compositional heterogeneity: Considerations for immunotherapy development. J Biol Chem **2021**;296:100057 doi 10.1074/jbc.REV120.013168.
37. Behrens LM, van Egmond M, van den Berg TK. Neutrophils as immune effector cells in antibody therapy in cancer. Immunol Rev **2022** doi 10.1111/imr.13159.
38. Ralston KS, Solga MD, Mackey-Lawrence NM, Somlata, Bhattacharya A, Petri WA, Jr. Trogocytosis by Entamoeba histolytica contributes to cell killing and tissue invasion. Nature **2014**;508(7497):526-30 doi 10.1038/nature13242.
39. Schmitz M, Zhao S, Schakel K, Bornhauser M, Ockert D, Rieber EP. Native human blood dendritic cells as potent effectors in antibody-dependent cellular cytotoxicity. Blood **2002**;100(4):1502-4.
40. Casneuf T, Xu XS, Adams HC, 3rd, Axel AE, Chiu C, Khan I, *et al.* Effects of daratumumab on natural killer cells and impact on clinical outcomes in relapsed or refractory multiple myeloma. Blood Adv **2017**;1(23):2105-14 doi 10.1182/bloodadvances.2017006866.
41. Wang Y, Zhang Y, Hughes T, Zhang J, Caligiuri MA, Benson DM, *et al.* Fratricide of NK Cells in Daratumumab Therapy for Multiple Myeloma Overcome by Ex Vivo-Expanded Autologous NK Cells. Clin Cancer Res **2018**;24(16):4006-17 doi 10.1158/1078-0432.CCR-17-3117.
42. Naeimi Kararoudi M, Nagai Y, Elmas E, de Souza Fernandes Pereira M, Ali SA, Imus PH, *et al.* CD38 deletion of human primary NK cells eliminates daratumumab-induced fratricide and boosts their effector activity. Blood **2020**;136(21):2416-27 doi 10.1182/blood.2020006200.
43. Krejcik J, Casneuf T, Nijhof IS, Verbist B, Bald J, Plesner T, *et al.* Daratumumab depletes CD38+ immune regulatory cells, promotes T-cell expansion, and skews T-cell repertoire in multiple myeloma. Blood **2016**;128(3):384-94 doi 10.1182/blood-2015-12-687749.
44. Krejcik J, Frerichs KA, Nijhof IS, van Kessel B, van Velzen JF, Bloem AC, *et al.* Monocytes and Granulocytes Reduce CD38 Expression Levels on Myeloma Cells in Patients Treated with Daratumumab. Clin Cancer Res **2017**;23(24):7498-511 doi 10.1158/1078-0432.CCR-17-2027.
45. Jin S, Sun Y, Liang X, Gu X, Ning J, Xu Y, *et al.* Emerging new therapeutic antibody derivatives for cancer treatment. Signal Transduct Target Ther **2022**;7(1):39 doi 10.1038/s41392-021-00868-x.
46. Coenon L, Villalba M. From CD16a Biology to Antibody-Dependent Cell-Mediated Cytotoxicity Improvement. Front Immunol **2022**;13:913215 doi 10.3389/fimmu.2022.913215.
47. Chu Y, Lamb M, Cairo MS, Lee DA. The Future of Natural Killer Cell Immunotherapy for B Cell Non-Hodgkin Lymphoma (B Cell NHL). Curr Treat Options Oncol **2022**;23(3):381-403 doi 10.1007/s11864-021-00932-2.
48. Wang B, Gallolu Kankanamalage S, Dong J, Liu Y. Optimization of therapeutic antibodies. Antib Ther **2021**;4(1):45-54 doi 10.1093/abt/tbab003.
49. Pereira NA, Chan KF, Lin PC, Song Z. The "less-is-more" in therapeutic antibodies: Afucosylated anti-cancer antibodies with enhanced antibody-dependent cellular cytotoxicity. MAbs **2018**;10(5):693-711 doi 10.1080/19420862.2018.1466767.
50. Chao MP, Takimoto CH, Feng DD, McKenna K, Gip P, Liu J, *et al.* Therapeutic Targeting of the Macrophage Immune Checkpoint CD47 in Myeloid Malignancies. Front Oncol **2019**;9:1380 doi 10.3389/fonc.2019.01380.

Figure Legends

Figure 1

slan$^+$-monocytes, but not NK cells, perform anti-CD47-dependent ADCC.

ADCC assays were performed using either slan$^+$-monocytes (**A**,**C**,**E**,**F**,**G**) or NK cells (**B**,**C**,**D**,**F**) cocultured for 4 h with Daudi cells, the latter cells either uncoated (black bars) or coated with: (**A**,**B**) 5 µg/ml RTX (white bars) and/or 1 or 5 µg/ml (light grey and grey bars, respectively) 5F9/Magrolimab (n=3-6); (**C**) 10 µg/mL anti-CD47 B6H12 mAbs (dotted bars, n=3); (**D**,**E**) 1-10 µg/ml anti-hCD20 IgG4 (white bars, n=3); (F) 1-10 µg/ml anti-CD47-hIgG1 mAbs (white bars, n=3); (**G**) 5 µg/ml RTX (white bars) or 5 µg/ml 5F9/Magrolimab (grey bars), in the presence or not of 10 µg/ml Certolizumab (n=9-12); (**H**) RTX (white bars) or 5F9/Magrolimab (grey bars) in the presence of either 10 µg/ml Z-VAD-FMK or 10 µMol NEC-1 (n=6-7). In (**A**-**F**, **H**), graphs show the percentages of Daudi cell cytotoxicity (means ± SEM) exerted by either slan$^+$-monocytes or NK cells, as determined by the Calcein AM release assay. In (**G**), graph shows the percentages of ADCC inhibition (means ± SEM) in the presence of Certolizumab. *$p < 0.05$; **$p < 0.01$; ***$p< 0.001$

Figure 2

Trogocytosis by slan$^+$-monocytes as determined by immunofluorescence microscopy.

Daudi cells were first labeled with MemBrite Fix Dye (in red), then coated with either RTX (**A**) or 5F9/Magrolimab (**B**), and finally co-incubated for 1 h with Calcein AM-labeled slan$^+$-monocytes (green cells), to be then analyzed by immunofluorescence microscopy. Two different fields were taken from the same slides (i.e., image #1 and #2). DAPI staining was used to detect cell nuclei (blue, in all panels). White arrows in panels I, III, IV and VI point to dots of red fluorescence corresponding to Daudi cell membranes acquired by slan$^+$-monocytes. Scale bars = 5 µm.

Figure 3

Trogocytosis by slan$^+$-monocytes as determined by flow cytometry.

(**A**,**B**) Representative flow cytometry plots displaying the gating strategy to identify trogocytosing (MDC8$^+$)slan$^+$-monocytes in coculture with uncoated, RTX- or 5F9/Magrolimab-coated Daudi cells for 1 h (**A**) and 4 h (**B**). Left panels of (**A**) and (**B**) display Sytox$^-$PKH26$^+$MDC8$^-$ Daudi cells (red cells) and (MDC8$^+$)slan$^+$-monocytes (purple cells). Middle panels of (**A**) and (**B**) show the expression of both PKH26 and CD16 by (MDC8$^+$)slan$^+$-monocytes (purple cells). Black gates include slan$^+$-monocytes performing trogocytosis (i.e., MDC8$^+$PKH26$^+$ cells) and indicate their

percentages. Right panels of (**A**) and (**B**) show the CD16 expression (as MFI values) by slan$^+$-monocytes. One representative experiment out of 9 is shown; (**C**,**D**) Graphs displaying the ADCC (**C**) and trogocytosis (**D**) levels (means ± SEM, n=5) performed by slan$^+$-monocytes after 1 and 4 h of coculture with Daudi cells; (**E**) Representative flow cytometry plots displaying the acquisition of CD19 and CD38 by slan$^+$-monocytes trogocytosing for 1 h. In left panels, MDC8$^+$PKH26$^+$ cells represent trogocytosing slan$^+$-monocytes. In middle and right panels, histogram overlays show CD19 and CD38 expression by PKH26$^+$slan$^+$-monocytes (darker histograms) and PKH26$^-$slan$^+$-monocytes (lighter histograms), as compared to their FMO (black dashed histograms); (**F**) CD19 and CD38 expression by uncoated (gray histograms), RTX- (dark purple histograms) or 5F9/Magrolimab (light purple histograms)-coated Daudi cells from the same cocultures shown in **E**. MFI values of CD19 by uncoated, RTX- or 5F9/Magrolimab-coated Daudi cells are, respectively, 14000, 3727 and 5612, while those of CD38 are 55539, 29166 and 34509. One representative experiment out of 9 is shown. *p < 0.05; **p < 0.01; ***p< 0.001

Figure 4

Effect of Certolizumab on trogocytosis by slan$^+$-monocytes

(**A**) Percentages of trogocytosing slan$^+$-monocytes cocultured with RTX- or 5F9/Magrolimab-coated Daudi cells for 1 h and 4 h, with or without 10 μg/ml Certolizumab (i.e., αTNFα antibodies)(means ± SEM, n=7); (**B**) Left panels show representative flow cytometry plots displaying PKH26$^+$MDC8$^-$ Daudi cells (red cells) and (MDC8$^+$) slan$^+$-monocytes (purple cells) cultured for 4 h with or without Certolizumab. Black gates include slan$^+$-monocytes performing trogocytosis (i.e., MDC8$^+$PKH26$^+$ cells) and indicate their percentages relative to Sytox$^-$,slan$^+$-monocytes. Right panels show the CD16 expression by slan$^+$-monocytes under the various coculture conditions (as MFI values). One representative experiment out of 7 is shown; (**C**) Representative flow cytometry plots displaying intracellular TNFα expression in cocultures of slan$^+$-monocytes (SSC^{low}MDC8$^+$ purple cells) with either RTX- or 5F9/Magrolimab-coated Daudi cells (SSC^{hi}MDC8$^-$ light blue cells) for 4 h. Contour plot overlays in middle and right panels show the expression of TNFα as compared to fluorescence FMO (gray contour plot), and illustrate that only slan$^+$-monocytes (i.e., SSC^{low}MDC8$^+$TNFα$^+$ cells) express TNFα (see black gates in middle panels including the related percentages). One representative experiment out of 3 is shown. **p < 0.01Pannello A. Le significativià vanno in fondo

Figure 5

slan$^+$-monocytes kill RTX/5F9-coated cancer cells by trogoptosis

Panels (**A**,**B**) display selected images taken from live cell imaging experiments (i.e., **Supplementary Video** 1 and 2) of slan$^+$-monocytes (unstained cells) incubated for 4 h with Daudi cells stained by intracellular Calcein AM (green fluorescence) and membrane PKH26 (red fluorescence) and coated with either RTX (**A**) or 5F9/Magrolimab (**B**). Green framed panels exemplify membrane destabilization of, and formation of blebs by, Daudi cells. Red framed panels exemplify trogocytosing slan$^+$-monocytes. Blue framed panels exemplify TO-PRO^{TM}-3 binding to cell nuclei (blue fluorescence), thus pointing to Daudi cell death. Panels framed in green, red and blue exemplify, respectively, membrane destabilization of, and formation of blebs by, Daudi cells; trogocytosing slan$^+$-monocytes; TO-PRO3^{TM} binding to cell nuclei (blue fluorescence), thus pointing to Daudi cell death. One representative experiment out of 3 performed is shown. Scale bars = 3 μm in panel A, 10 μm in panel B.

Figure 6

slan$^+$-monocytes perform Daratumumab-mediated trogoptosis

(**A**,**B**) Percentages of cytotoxicity exerted by slan$^+$-monocytes cocultured for 4 h with Daudi (**A**) or U266 (**B**) cell lines either uncoated (black bars) or coated (dotted bars) with 5 μg/ml DARA (mean ± SEM, n=5-12); (**C**) Graphs display the levels of trogocytosis performed by slan$^+$-monocytes after 1 h of coculture with DARA-coated Daudi cells; (**D**) immunofluorescence microscopy experiments of Daudi cells labeled with MemBrite Fix Dye (red cells), coated with DARA, and finally co-incubated with Calcein AM-labeled slan$^+$-monocytes (green cells) for 1 h. DAPI staining detect cell nuclei (blue, in all panels). White arrows in panels I and III point to dots of red fluorescence corresponding to Daudi cell membrane acquired by slan$^+$-monocytes; **(E, F)** Percentages of cytotoxicity exerted by slan$^+$-monocytes cocultured for 4 h with DARA-coated Daudi cells, in the absence or the presence of **(E)** either 25 μg/ml superoxide dismutase (SOD), or **(F)** 10 μg/mL Certolizumab (mean ± SEM, n=3); **(G)** Percentages of trogocytosing slan$^+$-monocytes cocultured with DARA-coated Daudi cells for 1 and 4 h, with or without 10 μg/ml Certolizumab (means ± SEM, n=4); **(H)** Panels display selected images taken from live cell imaging experiments (**Supplementary Video** 3) of slan$^+$-monocytes (unstained cells) incubated for 4 h with DARA-coated Daudi cells, exactly as described in Fig. 5. **p < 0.01; ***p< 0.001. Scale bars = 5 μm.

Figure 7

slan$^+$-monocytes perform RTX/5F9-mediated trogocytosis of neoplastic B cells

Representative flow cytometry plots displaying the gating strategy to identify trogocytosing ($MDC8^+$)$slan^+$-monocytes after 1 (**A**) and 4 h (**B**) of coculture with neoplastic B cells isolated from MCL lymph nodes. Left panels of (**A**) and (**B**) display $Sytox^-$, $PKH26^+MDC8^-$ neoplastic B cells (red cells) and ($MDC8^+$)$slan^+$-monocytes (purple cells). Black gates include $slan^+$-monocytes performing trogocytosis ($MDC8^+PKH26^+$ cells) and indicate their percentages relative to $Sytox^-$, $slan^+$-monocytes. Right panels show the CD16 expression by $slan^+$-monocytes (as MFI values). One representative experiment out of 5 is shown; (**C**) Bar graphs reporting the percentages of trogocytosing $slan^+$-monocytes after 1 h of coculture with neoplastic B cells from MCL, DLBCL, and FL (mean ± SEM, n=5); **D**) Representative flow cytometry plots displaying the acquisition of CD19 and CD38 by $slan^+$-monocytes trogocytosing B cells isolated from DLBCL lymph nodes for 1 h, as described in Fig. 3. One representative experiment out of 5 is shown; (**E**) Panels show sections from human FFPE tissue blocks of BL (panels I-II, n=2), double hit lymphoma (DHL, panels III, n=1), MCL (n=1, panel IV) and DLBCL relapse after RTX treatment (panels V-VII, n=1) stained with antibodies detecting the antigens indicated by labels. Yellow arrows point for examples of trogocytosis, as indicated by red dots of B cell markers present within the membrane of ($MDC8^+$/blue) $slan^+$-cells. Original magnification 80X. Scale bars = 33 μm (I-VII). *$p < 0.05$

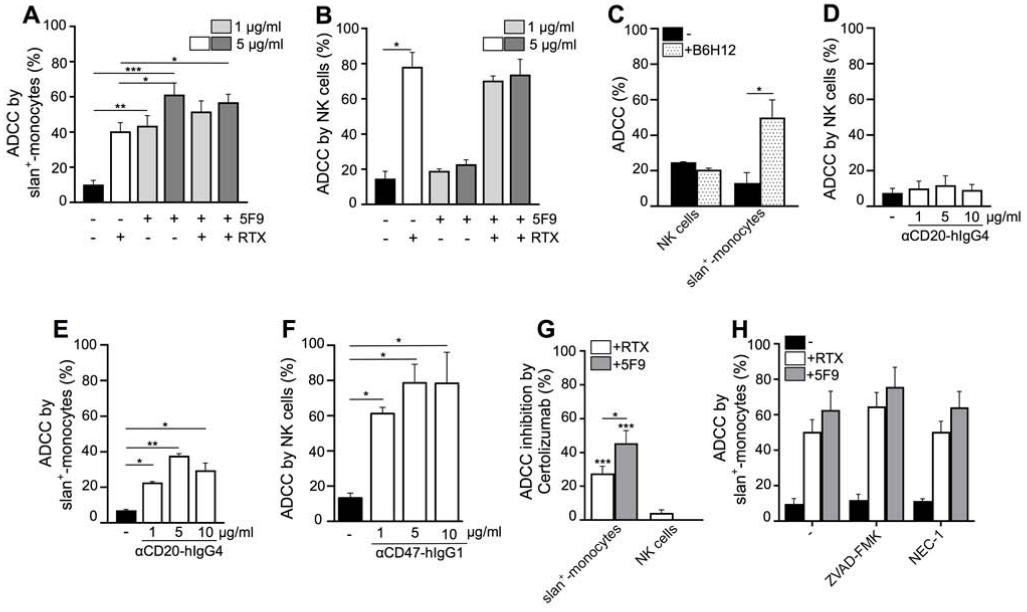
A
ADCC by slan+-monocytes (%)
1 µg/ml
5 µg/ml
- - + + + + 5F9
- + - - + + RTX
B
ADCC by NK cells (%)
1 µg/ml
5 µg/ml
- - + + + + 5F9
- + - - + + RTX
C
ADCC (%)
-
+B6H12
NK cells
slan+-monocytes
D
ADCC by NK cells (%)
- 1 5 10 µg/ml
αCD20-hIgG4
E
ADCC by slan+-monocytes (%)
- 1 5 10 µg/ml
αCD20-hIgG4
F
ADCC by NK cells (%)
- 1 5 10 µg/ml
αCD47-hIgG1
G
ADCC inhibition by Certolizumab (%)
+RTX
+5F9
slan+-monocytes
NK cells
H
ADCC by slan+-monocytes (%)
-
+RTX
+5F9
-
ZVAD-FMK
NEC-1

Figure 1

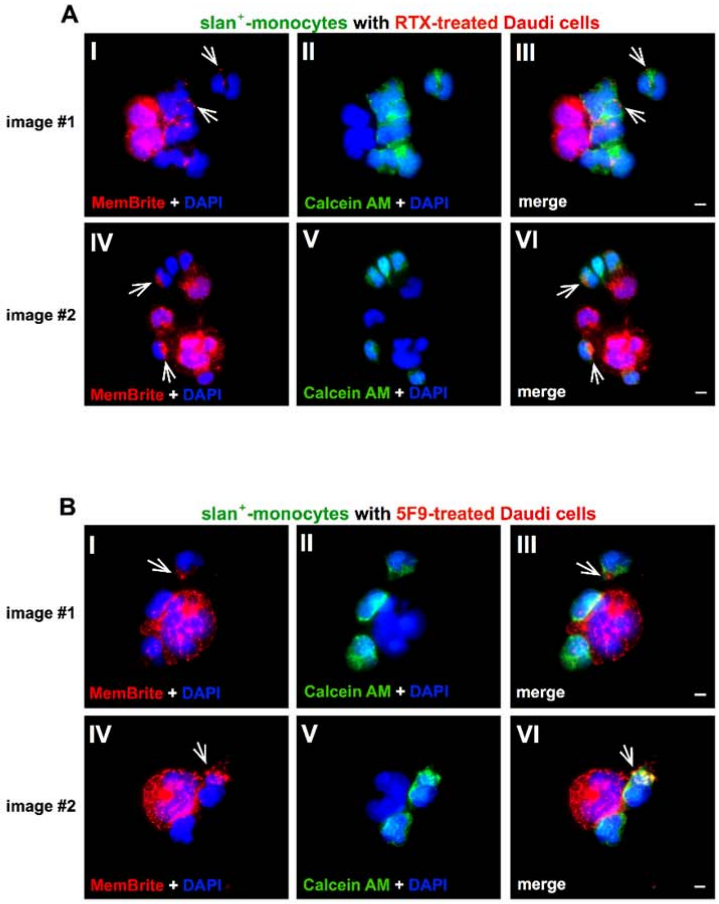
A
slan+-monocytes with RTX-treated Daudi cells
image #1
image #2
I
II
III
IV
V
VI
MemBrite + DAPI
Calcein AM + DAPI
merge
B
slan+-monocytes with 5F9-treated Daudi cells

Figure 2

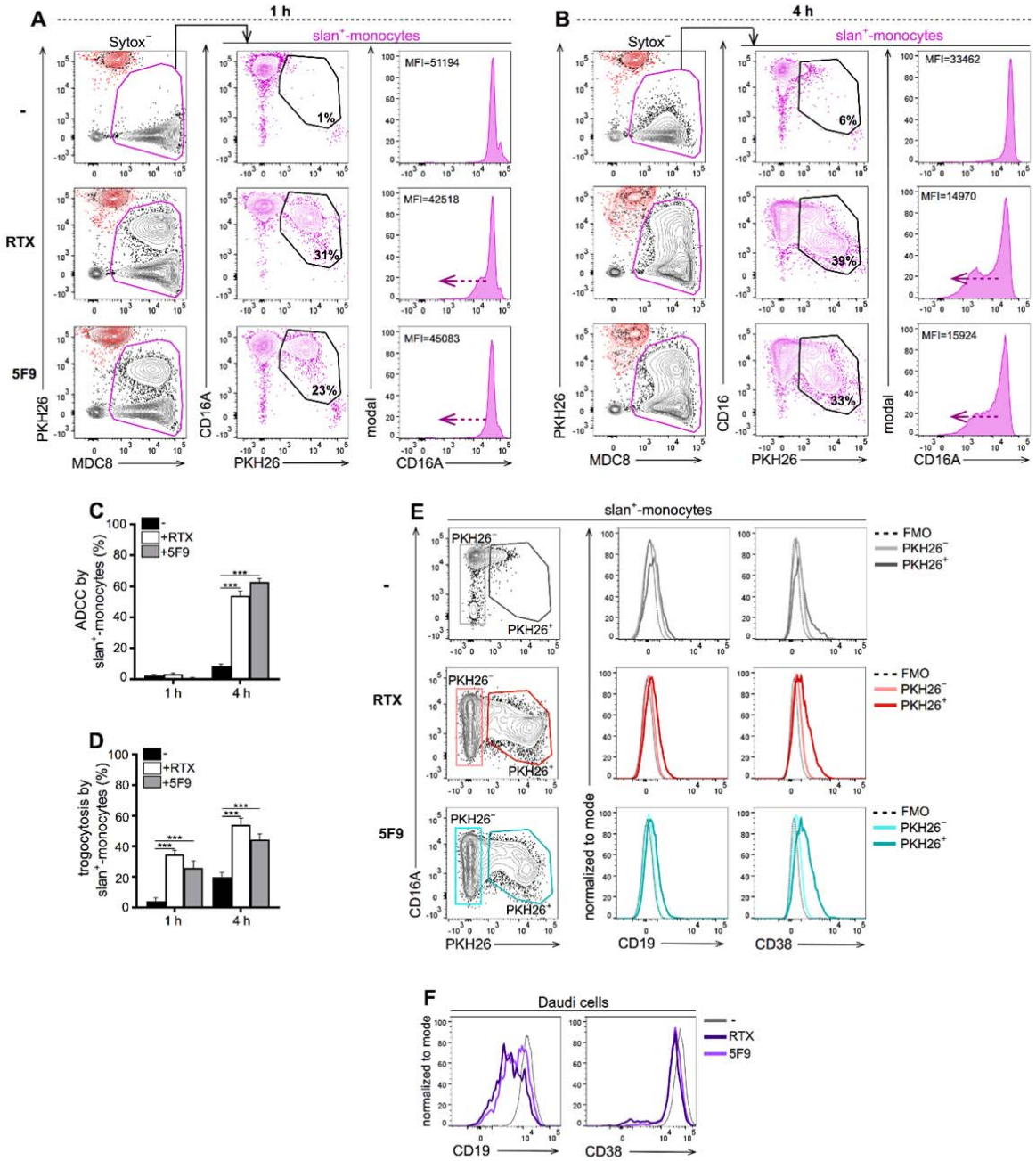
A
1 h
Sytox⁻
slan⁺-monocytes
-
RTX
5F9
1%
31%
23%
MFI=51194
MFI=42518
MFI=45083
PKH26
MDC8
CD16A
PKH26
modal
CD16A
B
4 h
Sytox⁻
slan⁺-monocytes
6%
39%
33%
MFI=33462
MFI=14970
MFI=15924
PKH26
MDC8
CD16
PKH26
modal
CD16A
C
-
+RTX
+5F9
ADCC by slan⁺-monocytes (%)
1 h
4 h
D
-
+RTX
+5F9
trogocytosis by slan⁺-monocytes (%)
1 h
4 h
E
slan⁺-monocytes
-
RTX
5F9
PKH26⁻
PKH26⁺
FMO
PKH26⁻
PKH26⁺
CD16A
PKH26
normalized to mode
CD19
CD38
F
Daudi cells
normalized to mode
-
RTX
5F9
CD19
CD38

Figure 3

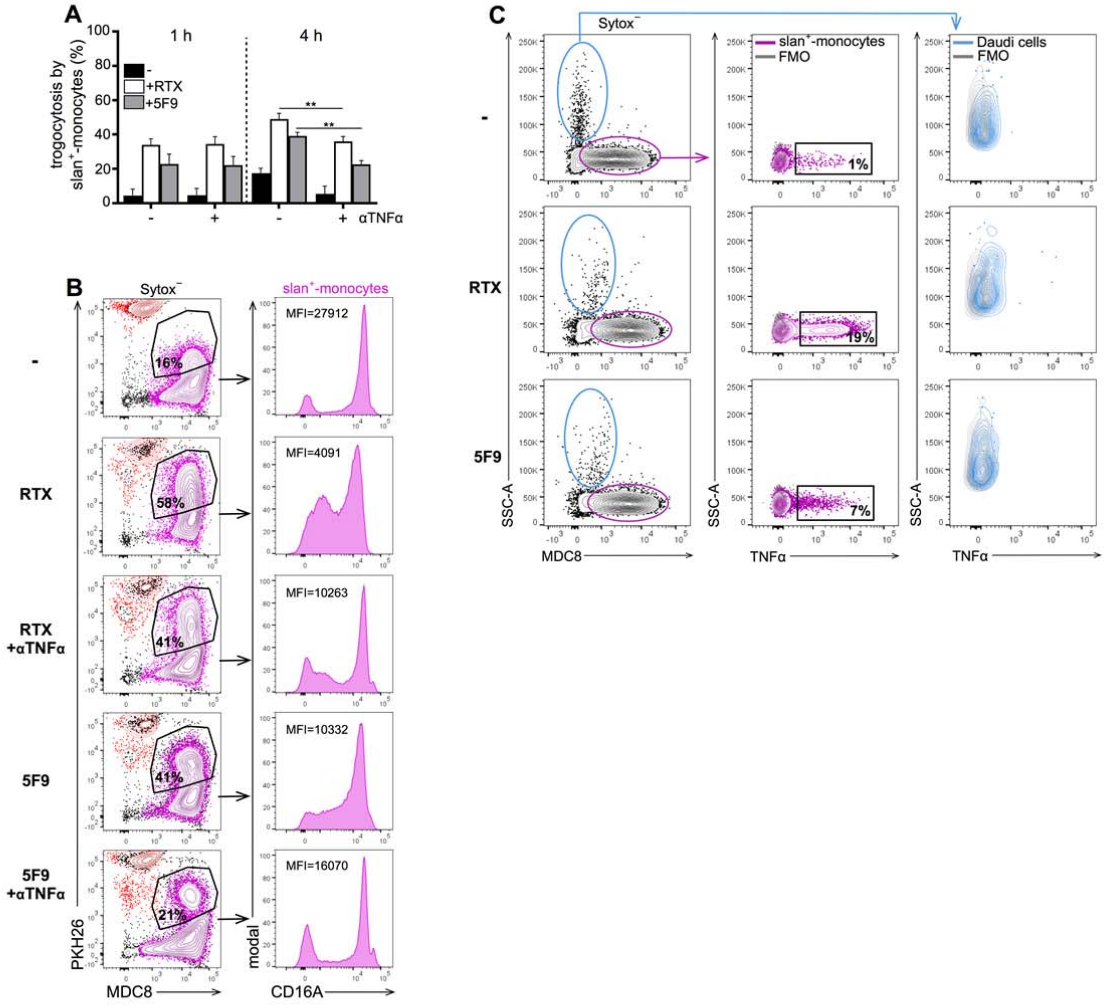
A
1 h
4 h
trogocytosis by slan+-monocytes (%)
-
+RTX
+5F9
**
**
αTNFα
B
Sytox−
slan+-monocytes
MFI=27912
MFI=4091
MFI=10263
MFI=10332
MFI=16070
16%
58%
41%
41%
21%
RTX
RTX +αTNFα
5F9
5F9 +αTNFα
PKH26
MDC8
modal
CD16A
C
Sytox−
slan+-monocytes
FMO
Daudi cells
FMO
1%
19%
7%
RTX
5F9
SSC-A
MDC8
TNFα
TNFα

Figure 4

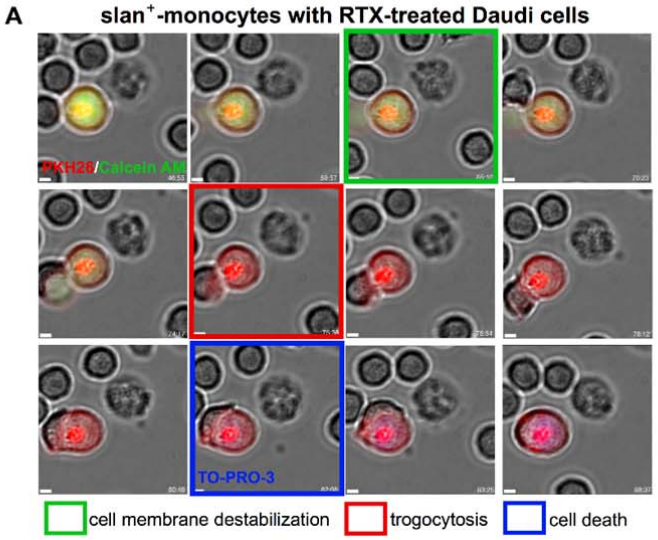
A
slan+-monocytes with RTX-treated Daudi cells
PKH26/Calcein AM
TO-PRO-3
cell membrane destabilization
trogocytosis
cell death
B
slan+-monocytes with 5F9-treated Daudi cells
PKH26/Calcein AM
TO-PRO-3
cell membrane destabilization
trogocytosis
cell death

Figure 5

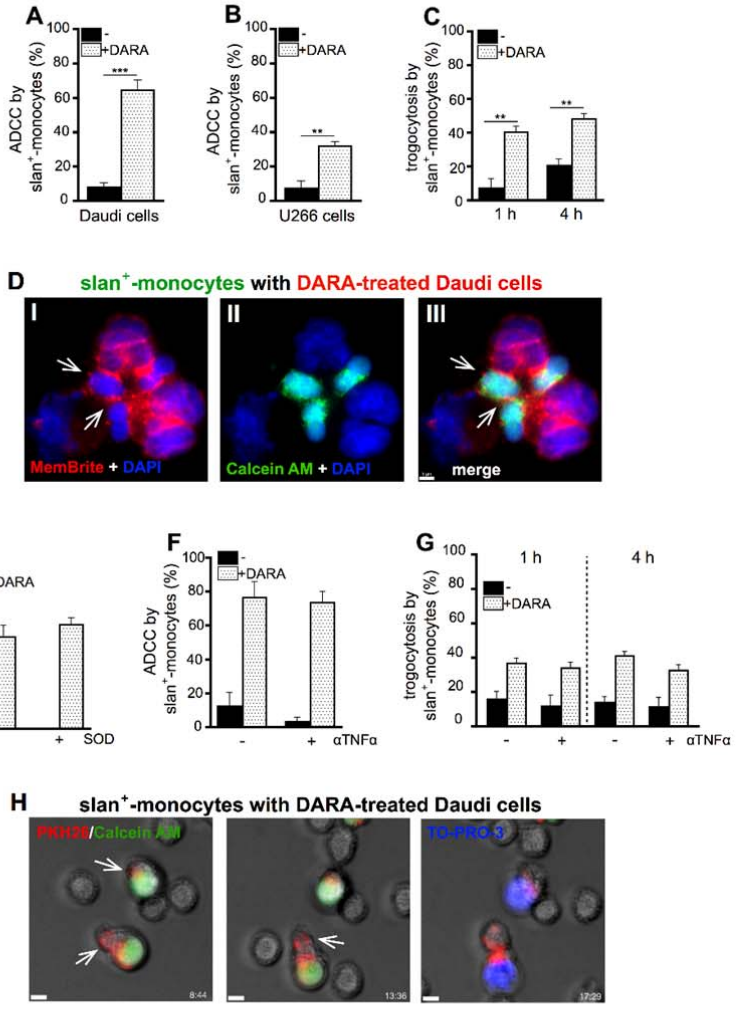
A
B
C
ADCC by slan+-monocytes (%)
trogocytosis by slan+-monocytes (%)
-
+DARA
***
**
Daudi cells
U266 cells
1 h
4 h
D
slan+-monocytes with DARA-treated Daudi cells
I
II
III
MemBrite + DAPI
Calcein AM + DAPI
merge
E
F
G
SOD
αTNFα
H
slan+-monocytes with DARA-treated Daudi cells
PKH26/Calcein AM
TO-PRO-3

Figure 6

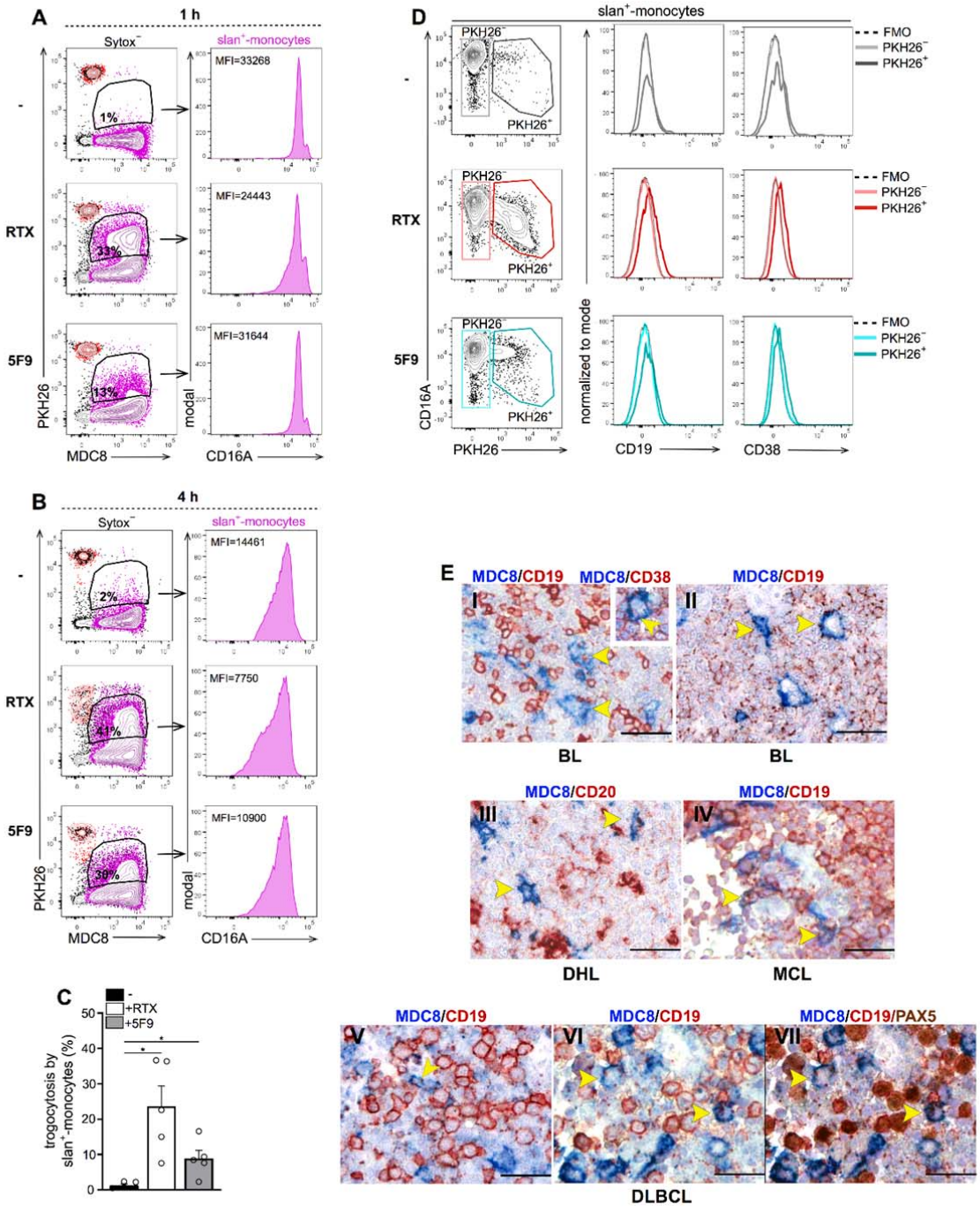
A
1 h
Sytox⁻
slan⁺-monocytes
-
RTX
5F9
1%
13%
13%
MFI=33268
MFI=24443
MFI=31644
PKH26
MDC8
CD16A
modal
B
4 h
2%
41%
30%
MFI=14461
MFI=7750
MFI=10900
C
-
+RTX
+5F9
trogocytosis by slan⁺-monocytes (%)
D
PKH26⁻
PKH26⁺
FMO
CD16A
CD19
CD38
normalized to mode
E
MDC8/CD19
MDC8/CD38
MDC8/CD20
MDC8/CD19/PAX5
I
II
III
IV
V
VI
VII
BL
DHL
MCL
DLBCL

Figure 7